

1

---

2  $\mu/\pi$  separation using

3 Convolutional Neural Networks

4 for the MicroBooNE

5 Charged Current Inclusive Cross Section

6 Measurement

---

7

8 Jessica Nicole Esquivel

9 Bachelor of Science in Electrical Engineering and Applied Physics

10 St. Mary's University

11 San Antonio, TX, USA 2011

12 DISSERTATION

13 Submitted in partial fulfillment

14 of the requirements for the degree

15 *Doctor of Philosophy in Physics*

16 - \* - DRAFT January 26, 2018 - \* -

17 December, 2017

18 Syracuse University

19 Syracuse, New York

20  
21  
22  
23

Copyright 2017  
Jessica Nicole Esquivel  
All Rights Reserved  
Syracuse University

24







## Abstract

The purpose of this thesis was to use Convolutional Neural Networks (CNN) to separate  $\mu's$  and  $\pi's$  for use in increasing the acceptance rate of  $\mu's$  below the implemented 75cm track length cut in the Charged Current Inclusive (CC-Inclusive) event selection for the CC-Inclusive Cross-Section Measurement. In doing this, we increase acceptance rate for CC-Inclusive events below a specific momentum range.



## Dedication

I dedicate this dissertation to the two important women in my life; My wife and my mom. Both have been there cheering me on giving me strength and love as I worked towards the hardest accomplishment I've ever done.

Jessica Nicole Esquivel





## Acknowledgements

38

39     Of the many people who deserve thanks, some are particularly prominent, such as  
40 my supervisor...



# 41 Contents



## <sup>42</sup> **List of figures**



## 43 **List of tables**





*“If the don’t give you a seat at the table,  
bring a folding chair.”*

— Shirley Chisholm



# Chapter 1

## Introduction

This thesis will be a description of work done to further increase efficiency and purity of the charged current inclusive cross section measurement using the MicroBooNE detector. It will also describe the MicroBooNE detector, what neutrinos are, the charged current inclusive cross section measurement and its importance as well as convolutional neural networks and how they can be used in  $\mu/\pi$  separation. Chapter 2 will talk about the background of neutrinos and the people and detectors that discovered neutrinos as well as an in depth history of neutrino oscillation and the discovery that neutrinos have mass.

Chapter 3 will discuss the MicroBooNE experiment, specifically, how Liquid Argon Time Projection Chambers work, the Light Collection System and the Electronic and Readout Trigger systems. This chapter will also describe the Booster Neutrino Beam stationed at Fermilab.

Chapter 4 will discuss the work that was done to detect the first neutrinos seen in the MicroBooNE detector and the software reconstruction efforts required to create an automated neutrino ID filter that was used to find the first neutrinos and then was later expanded on to create the charged current inclusive filter that will be discussed in chapter 5

Chapter ?? will give a brief description of what Convolutional Neural Networks are and how it will be used for  $\mu/\pi$  separation in this selection. Chapter ?? will discuss the hardware frameworks and training methods used to train multiple Convolutional Neural Networks for use in the charged current inclusive cross section measurement. Chapters ?? and ?? will discuss the results of using Convolutional Neural Networks on monte-carlo and data to sift out charged current inclusive neutrino events.



## Chapter 2

# Neutrinos

### 2.1 What are Neutrinos

Neutrinos are one of the fundamental particles which make up the universe. They are also one of the least understood. Neutrinos are not affected by the electromagnetic forces because they do not have electric charge. Neutrinos are affected by a "weak" sub-atomic force of much shorter range than electromagnetism, and are therefore able to pass through great distances in matter without being affected by it. Until the late 90's, neutrinos were thought to have no mass. Due to their mass, neutrinos are also affected by gravity. Neutrinos are created by radioactive decay or nuclear reactions such as the ones that happen in the sun, in nuclear reactors or when cosmic rays hit atoms. There are three types of neutrinos,  $\nu_e$ ,  $\nu_\mu$  and  $\nu_\tau$  which correspond to their charged lepton pairs.

As previously stated, neutrinos are very weakly interacting; in fact, neutrinos can pass unscathed through a wall of lead several hundred light-years thick. Because neutrinos interact so rarely, studying neutrinos requires a massive detector and a powerful neutrino source. With that being said, we can only infer their existence when they interact in a detector. In a collision, distinct charged particles are produced with each type of neutrino. An electron neutrino will create an electron, a muon neutrino will create a muon, and a tau neutrino will create a tau. The track the particle leaves in the detector is how one figures out what type of neutrino interaction was "seen". Liquid Argon Time Projection Chambers are the newest type of detectors being used to study neutrinos due to their excellent imaging and particle identification capabilities.

## 2.2 History of Neutrinos

The neutrino was first postulated by Wolfgang Pauli in 1931 to explain how beta decay could resolve the conservation of energy, momentum and angular momentum problem. Pauli suggested that this missing energy might be carried off, unseen, by a neutral particle (he called neutron) which was escaping detection. James Chadwick discovered a much heavier nuclear particle in 1932 that he also named neutron, leaving two particles with the same name. Enrico Fermi was the first person to coin the term neutrino (which means little neutral one in latin) in 1933 to fix this confusion. Fermi's paper, which was published in 1934, unified Pauli's neutrino with Paul Dirac's positron and Werner Heisenberg's neutron-proton model and his theory accurately explained many experimentally observed results. Wang Ganchang first proposed the use of beta capture to experimentally detect neutrinos and in 1959 Clyde Cowan and Frederick Reines published their work stating that they had detected the neutrino. The experiment called for antineutrinos created in a nuclear reactor by beta decay that reacted with protons producing neutrons and positrons:  $\nu_e + p^+ \rightarrow n^0 + e^+$ . Once this happens, the positron finds an electron and they annihilate each other and the resulting gamma rays are detectable. The neutron is detected by neutron capture and the releasing of another gamma ray. In 1962 Leon M. Lenderman, Melvin Schwartz and Jack Steinberger were the first to detect interactions of the muon neutrino. The first detection of the tau neutrino was announced in the summer of 2000 by the DONUT collaboration at Fermilab. In the late 1960s, many experiments found that the number of electron neutrinos arriving from the sun was around 1/3 to 1/2 the number predicted by the Standard Solar Model. This became known as the solar neutrino problem and remained unresolved for around thirty years. This problem was resolved by the discovery of neutrino oscillation and mass. [?]

## 2.3 Neutrino Oscillations

Neutrino oscillation was first predicted by Bruno Pontecorvo. It describes the phenomenon of a neutrino created with a specific lepton flavor (electron, muon or tau) that is later measured to have a different flavor. Neutrino oscillation is important theoretically and experimentally due to the fact that this observation implies that the neutrino has a non-zero mass, which is not part of the original Standard Model of particle physics. [?]

### 2.3.1 Solar Oscillations and the Solar Neutrino Problem

The solar neutrino flux derived from Bahcall's Standard Solar Model is shown in figure 2.1. Nuclear fusion and decay processes produce an abundant amount of neutrinos. The standard solar model predicts that these reactions produce several groups of neutrinos, each with differing fluxes and energy spectra. The figure also shows the ranges of detection of existing solar neutrino experiments in different shades of blue to illustrate that they sample different portions of the solar neutrino energy spectrum. Three of these experiments, plus a new one, are discussed below.

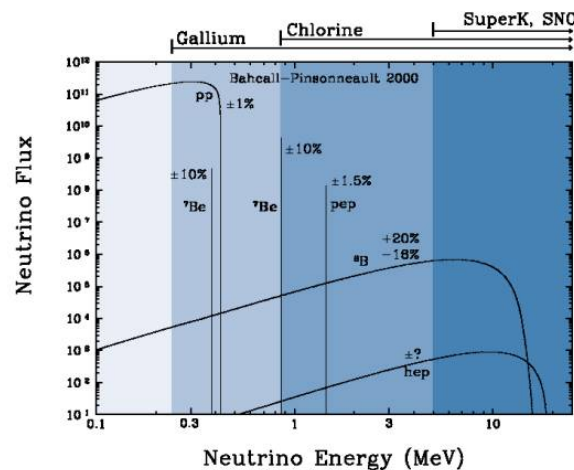


Figure 2.1: The Standard Solar Model

Since neutrinos rarely interact with matter, they pass through the sun and the earth undetected. About 65-billion neutrinos from the sun stream through every square centimeter on the Earth every second, yet we are oblivious to their passage in our every-day lives. [?]

The first experiment to detect the effects of neutrino oscillation was the Ray Davis's Homestake Experiment. The detector was stationed in the Homestake Gold Mine in Lead, South Dakota. It was 1,478 meters underground and was  $380 \text{ m}^3$ . The detector was filled with perchloroethylene. Perchloroethylene was chosen because of its high concentrations of chlorine. When an  $\nu_e$  interacted with chlorine-37 atom, the atom would transform to argon-37 which was then extracted and counted. The neutrino capture reaction is shown in equation 2.1. Davis observed a deficit of about 1/3 the flux of solar neutrinos that was predicted by Bahcall's Standard Solar Model.

146 The unexplained difference between the measured solar neutrino flux and model  
 147 predictions lead to the Solar Neutrino Problem. [?]



148 While it is now known that the Homestake Experiment detected neutrinos, some  
 149 physicist were weary of the results. Conclusive evidence of the Solar Neutrino Problem  
 150 was provided by the Kamiokande-II experiment, a water Cherenkov detector with  
 151 a low enough energy threshold to detect neutrinos through neutrino-electron elastic  
 152 scattering. In the elastic scattering interaction the electrons coming out of the point of  
 153 reaction strongly point in the direction that the neutrino was traveling, away from the  
 154 sun. While the neutrinos observed in Kamiokande-II were clearly from the sun, there  
 155 was still a discrepancy between Kamiokande-II and Homestake; The Kamiokande-  
 156 II experiment measured about 1/2 the predicted flux, rather than the 1/3 that the  
 157 Homestake Experiment saw.

158 The solution to the solar neutrino problem was finally experimentally determined  
 159 by the Sudbury Neutrino Observatory(SNO). The Ray Davis's Homestake Experiment  
 160 was only sensitive to electron neutrinos, and the Kamiokande-II Experiment was  
 161 dominated by the electron neutrino signal. The SNO experiment had the capability to  
 162 see all three neutrino flavors. Because of this, it was possible to measure the electron  
 163 neutrinos and total neutrino flux. The experiment demonstrated that the deficit was  
 164 due to the MSW effect, the conversion of electron neutrinos from their pure flavor  
 165 state into the second neutrino mass eigenstate as they passed through a resonance  
 166 due to the changing density of the sun. The resonance is energy dependent, and is  
 167 visible near 2MeV. The water cherenkov detectors only detect neutrinos above about  
 168 5MeV, while the radiochemical experiments were sensitive to lower energy (0.8MeV  
 169 for chlorine, 0.2MeV for gallium), and this turned out to be the source of the difference  
 170 in the observed neutrino rates at the two types of experiments. Figure 2.2 shows  
 171 Homestake, Kamiokande-II and SNO experiments.

## 172 MSW Effect

173 The Mikheyev-Smirnov-Wolfenstein effect is a process which acts to modify neu-  
 174 trino oscillations in matter. The presence of electrons in matter changes the energy



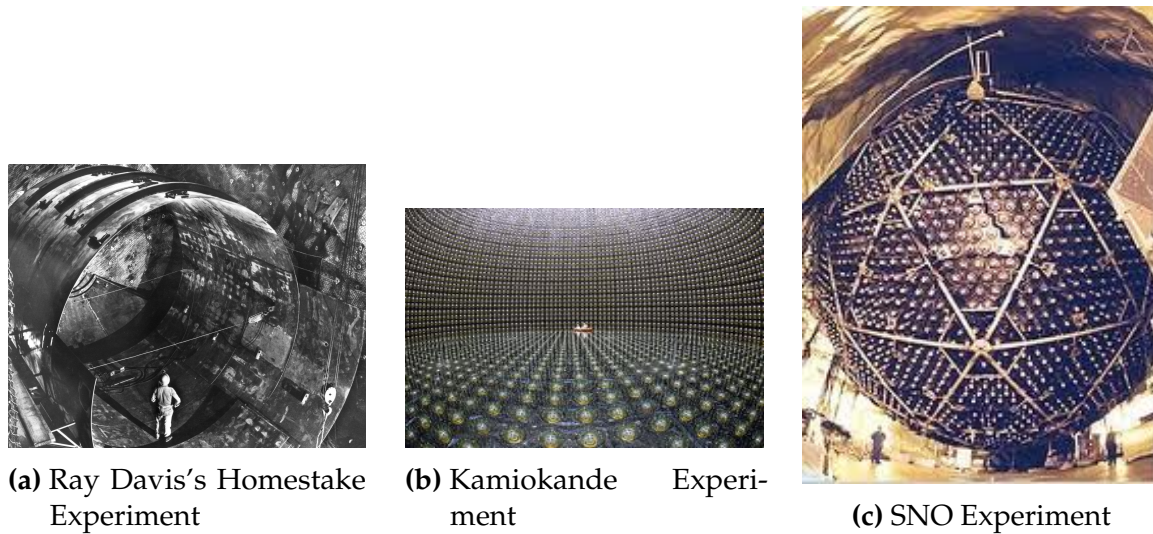


**Figure 2.2:** Solar Neutrino Experiments

levels of the mass eigenstates of neutrinos due to charged current coherent forward scattering of the electron neutrinos. This coherent forward scattering is similar to the electromagnetic process with respect to the refractive index of light in a medium. Because of this MSW Effect, neutrinos in vacuum have a different effective mass than neutrinos in matter and because neutrino oscillations depend on the squared mass difference of the neutrinos, the neutrino oscillations are different in matter than in vacuum. This effect is important at the sun where electron neutrinos are produced. The neutrinos of high energy leaving the sun are in a vacuum propagation eigenstate  $\nu_2$  that has a very small overlap with the electron neutrino  $\nu_e = \nu_1 \cos(\theta) + \nu_2 \sin(\theta)$  seen by the charged current reactions in Kamiokande-II and SNO. The discrepancy of the deficit between SNO, Kamiokande-II and Homestake is due to the energy of the solar neutrinos. The MSW effect "turns on" at about 2MeV and at lower energies, this MSW effect is negligible. [?]

### 2.3.2 Atmospheric Oscillations and the Atmospheric Neutrino Anomaly

Atmospheric neutrinos are neutrinos that stem from the decay hadrons coming from primary cosmic rays. The dominant part of the decay chain is shown in equations 2.2 and 2.3

$$\pi^+ \rightarrow \mu^+ \nu_\mu \mu^+ \rightarrow e^+ \nu_e \bar{\nu}_\mu \quad (2.2)$$

193

$$\pi^- \rightarrow \mu^- \bar{\nu}_\mu \mu^- \rightarrow e^- \bar{\nu}_e \nu_\mu \quad (2.3)$$

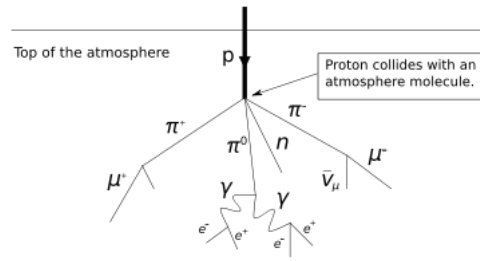


**Figure 2.3:** Cosmic Ray Shower

Figure 2.3 shows the cosmic ray shower. In general, these neutrinos have energies from 1GeV to 100s of GeV and the ratio of  $\nu_\mu$ s to  $\nu_e$ s equals to 2 (see equation 2.4)

$$R = \frac{(\nu_\mu + \bar{\nu}_\mu)}{(\nu_e + \bar{\nu}_e)} \quad (2.4)$$

There have been two types of detectors used to study atmospheric neutrinos: Water Cherenkov detectors and tracking calorimeters. Super-Kamiokande is the detector we will focus on. These atmospheric detector experiments measure the ratio of  $\nu_\mu$  to  $\nu_e$ . They also measure the zenith angle distribution of the neutrinos. These experiments report a double ratio (shown in equation 2.5). This double ratio is the ratio measured in the detector to the ratio that's expected which is 2. If the double ratio equals to 1, the data agrees with the prediction. Various measurements from multiple experiments are shown in figure 2.4. Except for Frejus, all R measurements are less than 1. This discrepancy between the predicted R and the measured R became known as the Atmospheric Neutrino Anomaly.

$$R = \frac{(N_\mu/N_e)_{DATA}}{(N_\mu/N_e)_{SIM}} \quad (2.5)$$

Kamiokande-II has the capability of measuring the direction of the incoming neutrinos. The expectation of atmospheric neutrino detection is that the flux be

Experiment	Type of experiment	R
Super-Kamiokande	Water Cerenkov	$0.675 \pm 0.085$
Soudan2	Iron Tracking Calorimeter	$0.69 \pm 0.13$
IMB	Water Cerenkov	$0.54 \pm 0.12$
Kamiokande	Water Cerenkov	$0.60 \pm 0.07$
Frejus	Iron Tracking Calorimeter	$1.0 \pm 0.15$

**Figure 2.4:** Measurements of the double ratio for various atmospheric neutrino experiments

isotropic due to the fact that atmospheric neutrinos can reach the detector from all directions. Kamiokande-II noticed that muon-like data did not agree well with this expectation. At low energies approximately half of the  $\nu_\mu$  are missing over the full range of zenith angles. At high energies the number of  $\nu_\mu$  coming down from above the detector seems to agree with expectation, but half of the same  $\nu_\mu$  coming up from below the detector are missing. This anomaly can be easily explained by neutrino flavor oscillations. Due to the fact that the neutrino travels less distance coming straight down into the detector (about 15km) than coming up from the bottom of the detector(13000km) changes the probability of oscillation. The probability of oscillation for the muon neutrinos coming down into the detector is roughly zero, whereas for neutrinos coming up, the oscillation probability is  $\sin^2(2\theta)$ . Both the solar and atmospheric neutrino problems can be explained by neutrino oscillation so its fitting to derive this phenomenon mathematically. In the next two sections, two flavor and three flavor neutrino oscillation derivations will be explained.

### 2.3.3 Two Flavor Neutrino Oscillation Formulation

The flavor eigenstates can oscillate between eachother because they are composed of an add-mixture of mass eigenstates( $\nu_1, \nu_2$ ). Figure 2.5 shows the mass and flavor eigenstates rotated by an angle  $\theta$  which is the mixing angle.

In matrix form the wavefunctions are:

$$\begin{pmatrix} \nu_\mu \\ \nu_e \end{pmatrix} = \begin{pmatrix} \cos\theta & \sin\theta \\ -\sin\theta & \cos\theta \end{pmatrix} * \begin{pmatrix} \nu_1 \\ \nu_2 \end{pmatrix} \quad (2.6)$$

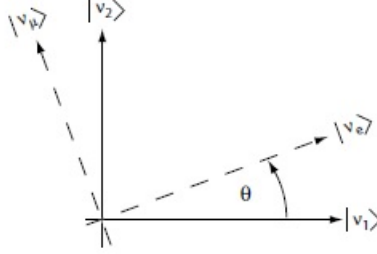


**Figure 2.5:** The flavor eigenstates are rotated by an angle  $\theta$  with respect to the mass eigenstates

227 Applying the time evolution operator to  $\nu_\mu$ :

$$|\nu_\mu(t)\rangle = -\sin\theta|\nu_1\rangle e^{-i\frac{E_1 t}{\hbar}} + \cos\theta|\nu_2\rangle e^{-i\frac{E_2 t}{\hbar}} \quad (2.7)$$

228 where  $E_1 = \sqrt{p^2 c^2 + m_1^2 c^4}$  and  $E_2 = \sqrt{p^2 c^2 + m_2^2 c^4}$  and  $p_1 = p_2$ . For the time  
 229 being, let us assume  $\hbar = c = 1$ . With this assumption:  $E_1 = \sqrt{p^2 + m_1^2}$  and  $E_2 =$   
 230  $\sqrt{p^2 + m_2^2}$ . The next modifications is to assume neutrinos are relativistic:

$$\gamma = \frac{E}{m_0 c^2} = \frac{\sqrt{p^2 c^2 + m_0^2 c^4}}{m_0 c^2} \gg 1 \quad (2.8)$$

231 because of this,

$$p \gg m_0 \quad (2.9)$$

232

$$E = \sqrt{p^2 + m_0^2} = p \sqrt{1 + m_0^2/p^2} \simeq p + \frac{1}{2} \frac{m_0^2}{p} \quad (2.10)$$

233 where the binomial expansion is used. Now  $E_1$  and  $E_2$  can be written as:

$$E_1 \simeq p + \frac{1}{2} \frac{m_1^2}{p} \text{ and } E_2 \simeq p + \frac{1}{2} \frac{m_2^2}{p} \quad (2.11)$$

234 Now applying all these assumptions back into equation 2.7 gives us:

$$|\nu_\mu(t)\rangle = -\sin\theta|\nu_1\rangle e^{-i\left(p + \frac{1}{2} \frac{m_1^2}{p}\right)t} + \cos\theta|\nu_2\rangle e^{-i\left(p + \frac{1}{2} \frac{m_2^2}{p}\right)t} \quad (2.12)$$

$$|\nu_\mu(t)\rangle = e^{-i\left(p + \frac{1}{2}\frac{m_1^2 - m_2^2}{p}\right)t} (-\sin\theta|\nu_1\rangle + \cos\theta|\nu_2\rangle) \quad (2.13)$$

235 Substituting  $\Delta m^2 = m_1^2 - m_2^2$  and  $t = \frac{x}{c} = x$  and  $e^{-iz} = e^{-i\left(p + \frac{1}{2}\frac{m_1^2}{p}\right)t}$  gives us:

$$|\nu_\mu(t)\rangle = e^{-iz} \left( -\sin\theta|\nu_1\rangle + \cos\theta|\nu_2\rangle e^{+ix\left(\frac{1}{2}\frac{\Delta m^2}{p}\right)} \right) \quad (2.14)$$

236 Finding the Probability for a  $\nu_\mu \rightarrow \nu_e$ :

$$P(\nu_\mu \rightarrow \nu_e) = |\langle \nu_e | \nu_\mu(t) \rangle|^2 \quad (2.15)$$

237 Remembering that  $\langle \nu_i | \nu_j \rangle = \delta_{ij}$

$$\langle \nu_e | \nu_\mu(t) \rangle = e^{-iz} \left( -\sin\theta\cos\theta + \sin\theta\cos\theta e^{\frac{i\Delta m^2 x}{p}} \right) \quad (2.16)$$

238 Taking the absolute value squared gives us:

$$P(\nu_\mu \rightarrow \nu_e) = |\langle \nu_e | \nu_\mu(t) \rangle|^2 = e^{+iz} e^{-iz} \sin^2\theta \cos^2\theta \left( -1 + e^{\frac{i\Delta m^2 x}{p}} \right) \left( -1 + e^{\frac{i\Delta m^2 x}{p}} \right) \quad (2.17)$$

239 Since the neutrino is relativistic we can set  $p = E_\nu$  and change  $x = L$ . Also  
 240 recognizing the trigonometric relation  $(1 - \cos 2\theta)/2 = \sin^2\theta$  the above equation  
 241 becomes:

$$P(\nu_\mu \rightarrow \nu_e) = \sin^2 2\theta \sin^2 \left( \frac{\Delta m^2 L}{4E_\nu} \right) \quad (2.18)$$

242 All that's left to do now is re-introduce  $\hbar$  and  $c$  doing this we get:

$$P_{\nu_\mu \rightarrow \nu_e}(L, E) = \sin^2 2\theta \sin^2 \left( 1.27 \Delta m^2 \frac{L}{E_\nu} \right) \quad (2.19)$$

243 This equations has three important variables.

- The angle  $\theta$ : This angle, as mentioned before, is called the mixing angle. It defines the difference between the flavor and the mass eigenstates. When  $\theta = 0$  the mass and flavor eigenstates are identical and now oscillations occur.
- The mass squared difference,  $\Delta m^2$ : Again  $\Delta m^2 = m_1^2 - m_2^2$ . The reason this is an important variable is because it implies that for neutrinos to oscillate, neutrinos must have mass. Furthermore, the mass squared difference also tells us that the neutrino mass eigenstates must be different.
- L/E: This is the variable that is of most interest to experimental physicists due to the fact that it is the variable that we set. L is the distance between the source and detector and E is the energy of the neutrino. For a given  $\Delta m^2$ , the probability of oscillation changes with respect to L/E.

### 2.3.4 Three Flavor Neutrino Oscillation Formulation

Seeing the quantum mechanics involved in deriving the probability of a two flavor neutrino oscillation, it is now possible to formulate the three flavor neutrino oscillation. The three flavor neutrino oscillation formulation begins similarly to the two flavor, but there is the Pontecorvo-Maki-Nakagawa-Sakata matrix (PMNS) instead of the 2X2 matrix in the previous section. The PMNS matrix is show below:

$$\begin{pmatrix} c_{12}c_{13} & s_{12}c_{13} & s_{13}e^{-i\delta} \\ -s_{12}c_{23} - c_{12}s_{23}s_{13}e^{i\delta} & c_{12}c_{23} - s_{12}s_{23}s_{13}e^{i\delta} & s_{23}c_{13} \\ s_{12}s_{23} - c_{12}c_{23}s_{13}e^{i\delta} & -c_{12}s_{23} - s_{12}c_{23}s_{13}e^{i\delta} & c_{23}c_{13} \end{pmatrix} * \begin{pmatrix} e^{i\alpha_1/2} & 0 & 0 \\ 0 & e^{i\alpha_2/2} & 0 \\ 0 & 0 & 1 \end{pmatrix} \quad (2.20)$$

where  $c_{ij} = \cos\theta_{ij}$  and  $s_{ij} = \sin\theta_{ij}$

Following the same steps as before we get:

$$P_{\alpha \rightarrow \beta} = \delta_{\alpha\beta} - 4\sum \text{Re}(U_{\alpha i}^* U_{\beta i} U_{\alpha j} U_{\beta j}^*) \sin^2 \left( \frac{\Delta m_{ij}^2 L}{4E} \right) + 2\sum \text{Im}(U_{\alpha i}^* U_{\beta i} U_{\alpha j} U_{\beta j}^*) \sin \left( \frac{\Delta m_{ij}^2 L}{2E} \right) \quad (2.21)$$

The main things to notice here are  $\delta_{ij}$  which is the CP violating term and has not been measured yet, and  $\theta_{13}$  which has just been measured. CP violation is a violation

of the postulated CP-symmetry. CP-symmetry states that the laws of physics should be the same if a particle were to be exchanged with its antiparticle and then if the left hand side of a decay were switched with the right hand side.

### 2.3.5 Reactor Oscillation

Many experiments have searched for oscillation of electron anti-neutrinos produced at nuclear reactors. Such oscillations give the value of the parameter  $\theta_{13}$ . The KamLAND experiment, started in 2002, has made a high precision observation of reactor neutrino oscillation. Neutrinos produced in nuclear reactors have energies similar to solar neutrinos, a few MeV. The baselines of these experiments have ranged from tens of meters to over 100 km. On 8 March 2012, the Daya Bay team announced a  $5.2\sigma$  discovery that  $\theta_{13} \neq 0$ .





## Chapter 3

# The MicroBooNE Experiment

The purpose of this chapter is to discuss and understand the details of the MicroBooNE detector. A thorough understanding of MicroBooNE and the technology behind liquid argon time projection chambers is important for understanding results as well as understanding how images were made for use in deep learning efforts that will be outlined in later chapters.

### 3.1 Liquid argon time projection chambers

Liquid Argon Time Projection Chambers (LArTPCs) are an exciting detector technology that provide excellent imaging and particle identification, and are now being used to study neutrinos. The Time Projection Chamber (TPC) was first invented by Nygren in 1974 [?] and the proposal for a LArTPC for neutrino physics was made by Rubbia [?] in 1977 with the ICARUS collaboration implementing this concept [?]. A LArTPC is a three-dimensional imaging detector that uses planes of wires at the edge of an active volume to read out an interaction. When a neutrino interacts with an argon atom, the charged particles that are produced ionize the LAr as they travel away from the interaction. By placing a uniform electric field throughout the LAr volume, the ionization is made to drift towards a set of anode planes, which consist of wires spaced very closely together collecting the ionized charge, which is subsequently read out by electronics connected to the anode wires. The collected ionization creates a spatial image of what happened in the detector on each anode plane. The position resolution of the interaction along the beam direction (perpendicular to drift direction) relies on the wire pitch, while the resolution in drift direction is dependent on the

timing resolution of the electronics used and the longitudinal diffusion in the volume. The drift time of the ionization relative to the time of the original signal allows the signal to be projected back along the drift coordinate, hence the name LArTPC. Having very small distances between each wire within an anode plane allows for very fine granularity and detail to be captured, and having multiple wire planes at different angles provides independent two-dimensional views that can be combined into a three dimensional picture of the interaction. Once the charge signal is created on the anode planes, software analysis packages identify particles in the detector by using deposited energy on the wires along their track length. The 30 year development of the ICARUS detector has led to LArTPCs being used as cosmic ray [?], solar neutrino [?] and accelerator neutrino [?] detectors. The ArgoNeuT experiment at Fermilab was the first United States based liquid argon neutrino program that has since produced short-baseline  $\nu - Ar$  cross-section measurements in the NUMI beamline [?]. The MicroBooNE experiment is the second experiment in the US based LArTPC neutrino program and will be discussed thoroughly in the next sections. The next phases of the liquid argon neutrino program are under way and are the Fermilab Short Baseline Neutrino (SBN) program [?] and the Deep Underground Neutrino Experiment (DUNE) [?]. The SBN program will include three LArTPC detectors, including the MicroBooNE detector, on the Booster Neutrino Beam (BNB) to do multiple-baseline oscillation measurements. The detector closest to the beam will be the 40 ton Short Baseline Neutrino Detector (SBND) [?] at 150 m and the detector furthest is the 600 ton ICARUS T600 [?] detector positioned at 600 m. The DUNE collaboration will deliver a 30 GeV neutrino beam 1300 km from Fermilab to a 34 kiloton LArTPC detector at Homestake, SD. DUNE will study the leptonic CP phase,  $\delta_{cp}$ , as well as measure neutrino and antineutrino oscillations.

## 3.2 The MicroBooNE Time Projection Chamber

MicroBooNE (Micro Booster Neutrino Experiment) is a 89 ton active volume (180 ton total mass) LArTPC which is then inserted into a cylindrical cryostat on axis of the Booster Neutrino Beam (BNB) stationed at Fermilab in Batavia, Illinois. Understanding LArTPC technology and detector physics is necessary to build a LArTPC the size of DUNE, and MicroBooNE has made many advances in developing this technology [?].

MicroBooNE's Time Projection Chamber (TPC) is 10.3 m long (beamline direction), 2.3 m high and 2.5 m wide (which corresponds to the drift distance). The TPC is shown in figure ???. MicroBooNE is the largest LArTPC currently running in the world [?]. This LArTPC has 3 wire planes: 1 plane that collects the ionization in the wires and is  $0^\circ$  to the vertical with 3456 wires spaced 3 mm apart, and 2 planes where the ionization drifts passed and induces a signal at  $\pm 60^\circ$  to the vertical each with 2400 wires also spaced 3 mm apart. Each plane has a spacing also of 3 mm from each other. The first two planes are the induction planes and the last is the collection. The 270 V/cm electric field of the TPC is created using 64 stainless steel tubes shaped into rectangles around the TPC and held in place by G10 to form a field cage. The cathode is charged at a high voltage of -70 kV and this voltage is stepped down across the field cage tubes using a voltage divider chain with an equivalent resistance of 240 M $\Omega$  between the tubes. The field cage tubes are separated by 4 cm from center to center. The electron drift distance is 2.5 m in the x direction with a drift time of 2.3 ms. Maintaining high charge yield is done by continuously recirculating and purifying the argon. The purity is monitored using MicroBooNE's light collection system. Another use of the light collection system is initial timing and drift coordinate of the interaction.

MicroBooNE's light collection system is a crucial part for 3D reconstruction of all particle interactions in the LArTPC. The initial interaction time,  $t_0$ , and initial drift coordinate,  $x_0$ , are not known from the TPC alone. For beam events, the accelerator clock is used to determine  $t_0$  of the interaction and the  $x_0$  can be inferred using drift time. Non-beam events, however, do not have this capability, which is why scintillation light from an interaction is used. The  $\nu - Ar$  interaction produces scintillation light which is collected by photomultiplier tubes (PMTs) which allows the exact time,  $t_0$  of the neutrino interaction to be determined. The scintillation light created propagates within nanoseconds to the light collection system compared to the milliseconds it takes the ionized electrons from the interaction to reach the anode wire planes. Therefore we can precisely know where along the drift direction the particle interaction first took place. The scintillation light is also localized, so combining the PMT information with the wire plane information allows for cosmic background rejection happening outside the beam timing window.

The light collection system is made up of 32 Hamamatsu R5912-02mod cryogenic PMTs with a diameter of 8-inches. The PMTs are located behind the 3 wire anode planes and provides 0.85% photocathode coverage. Each PMT has an acrylic plate mounted in front of it that is coated with a wave-length shifting material called TPB.

The acrylic plates take in the scintillation light, at 128 nm, and re-emits it visible wavelengths visible to the PMTs, with a peak at 425 nm.

Both the light collection system and the TPC create analog signal that is read out and digitized by the electronics system. The process requires amplification and shaping of the signal which then is goes to the data aquisition (DAQ) software for writing of the digitized data to disk. The anode plane wires are connected to detector specific circuit boards (ASICS) that are submerged and operate inside the liquid argon volume. These ASICS send amplified signal to 11 feed-throughs where further amplification of the signal happens outside the cryostat. The signal is received by custom LArTPC readout modules distributed over nine readout crates which do the digitization. The TPC wires are digitized at 16 MHz then downsampled to 2 MHz. The TPC system reads out 4 frames of wire signal data per event, 1 frame before a trigger and 2 frames after the triggered frame. The four frames allows for identification of a neutrino interaction as well as cosmic background rejection. The process of digitization is similar for the light collection system. Each PMT signal undergoes a shaping with a 60 ns peaking time for digitization of multiple samples. The digitization occurs at 64 MHz but are not read out continuously during the TPC readout time. Only shaped PMT signal samples above a small threshold are read out and saved. Both the TPC and PMT readouts are initiated via triggers on a separate trigger board located in a warm electronics crate. The timing trigger is created by a timing signal from the BNB accelerator which is shaped and sent to the trigger board. The PMT trigger is generated when the PMT signal multiplicity is greater than 1 and the summed PMT pulse-height is more than 2 photo-electrons summed up over all PMT channels. When the trigger board gets both a timing trigger and a PMT trigger in coincidence, a BNB trigger is then generated by the board. This signal is then passed to all readout crates initiating the readout of data. The data is then sent to the DAQ software which then saves the data to disk into one event memory.

### 3.3 MicroBooNE's Physics Goals

#### 3.3.1 The low-energy excess

The primary goal of the MicroBooNE experiment is to study and investigate the low-energy excess seen in MiniBooNE [3.1](#). MicroBooNE has the capability of confirming or

denying this excess as electrons or photons due to the detector being in the same beam, having a similar baseline, and lastly the detector being able to clearly distinguish between electrons and photons. LArTPCs use the topology of events as well as energy loss near the vertex to differentiate between single  $e^-$  tracks and photon-induced induced pair production  $\gamma \rightarrow e^+ e^-$ , which wasn't possible in MiniBooNE, a Cherenkov detector. This technique has been shown in the ArogoNeuT detector [?] and a side by side comparison of both event types in a LArTPC can be seen in figure ?? . An excess in electrons would point towards new oscillation physics beyond the standard model, while photons would be within the standard model. MicroBooNE will observe a 4-5 $\sigma$  signal.

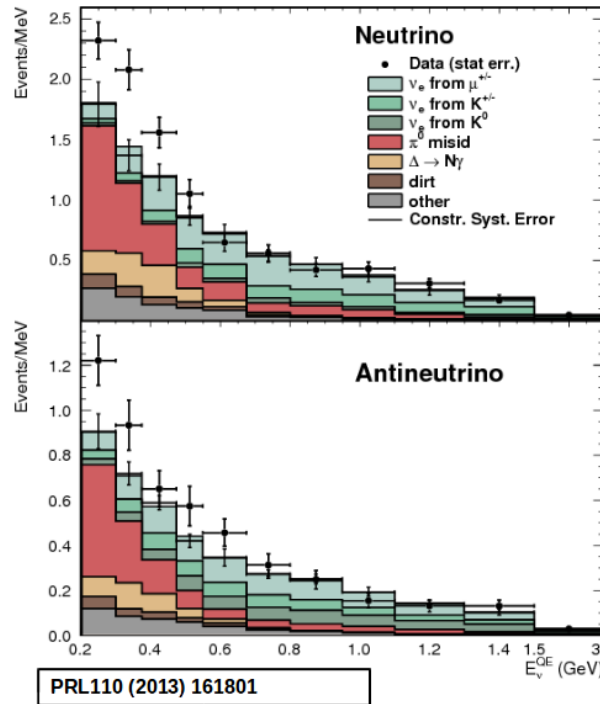


Figure 3.1: Low Energy excess seen in MiniBooNE

### 3.3.2 Cross sections

MicroBooNE's neutrino cross-section program will be the first  $\nu - Ar$  cross-section in the 1 GeV energy range and one of only a few cross-section measurements of  $\nu - Ar$  in the world. MicroBooNE is also the first liquid argon detector to collect the highest statistics sample of neutrino interactions. Investigating final-state-interactions in the 1GeV energy range provides information about short range nuclear correlations that affect the interpretations of neutrino oscillation experiment data.

One of the cross-section measurements MicroBooNE can make is an inclusive charged-current cross-section measurement (referred to as CC-inclusive). CC-inclusive events consist of a neutrino exchanging a  $W^\pm$  boson with an argon atom, producing a charged lepton and any number of other final state particles. In MicroBooNE's case, a CC-inclusive event will mostly have a defining muon track coming out of the vertex due to our neutrinos being predominately  $\nu_\mu$ s. A cross-section measurement is the energy dependent probability of  $\nu - Ar$  interaction in the detector. Cross-sections however are independent of the intensity or focus of the particle beam so they can be compared among different experiments. A background for a CC-inclusive cross-section measurement are the neutral-current events that contain a pion. It is possible to have a neutral current interaction with a  $\pi + p$  event signature that looks like a charged current  $\mu + p$  event. Reconstruction tools implemented to date don't efficiently separate muons from pions. A common way to separate these two particles species is to implement a track length cut. On average, muons tend to have longer track lengths in LArTPCs so by requiring that the hypothesized lepton be above a threshold track length, it is possible to increase signal to background.

### 3.3.3 Liquid argon detector development

The last physics goal for the MicroBooNE collaboration is to provide important information regarding LArTPC technology. Being the first in large scale LArTPCs in the US, MicroBooNE will be able to provide improvements to High Voltage (HV) distribution, Noise Characterization [?], and Michel Electron Reconstruction [?].

## 3.4 The Booster Neutrino Beam

The MicroBooNE detector is stationed at Fermi National Accelerator Laboratory (FNAL) where it receives neutrinos from both the Booster Neutrino Beam (BNB) and Neutrinos from the Main Injector (NuMI) beams. MicroBooNE is on-axis for the BNB and off-axis by 135 mrad for NuMI. For the purpose of this analysis, only data from the BNB was used. This section will discuss how neutrinos are created using the BNB. How these neutrinos are produced as well as their flux through the MicroBooNE detector is necessary for any analysis because of the systematic uncertainties the beam

introduces to a measurement. An arial view of fermilab as well as the BNB is shown in figure 3.2

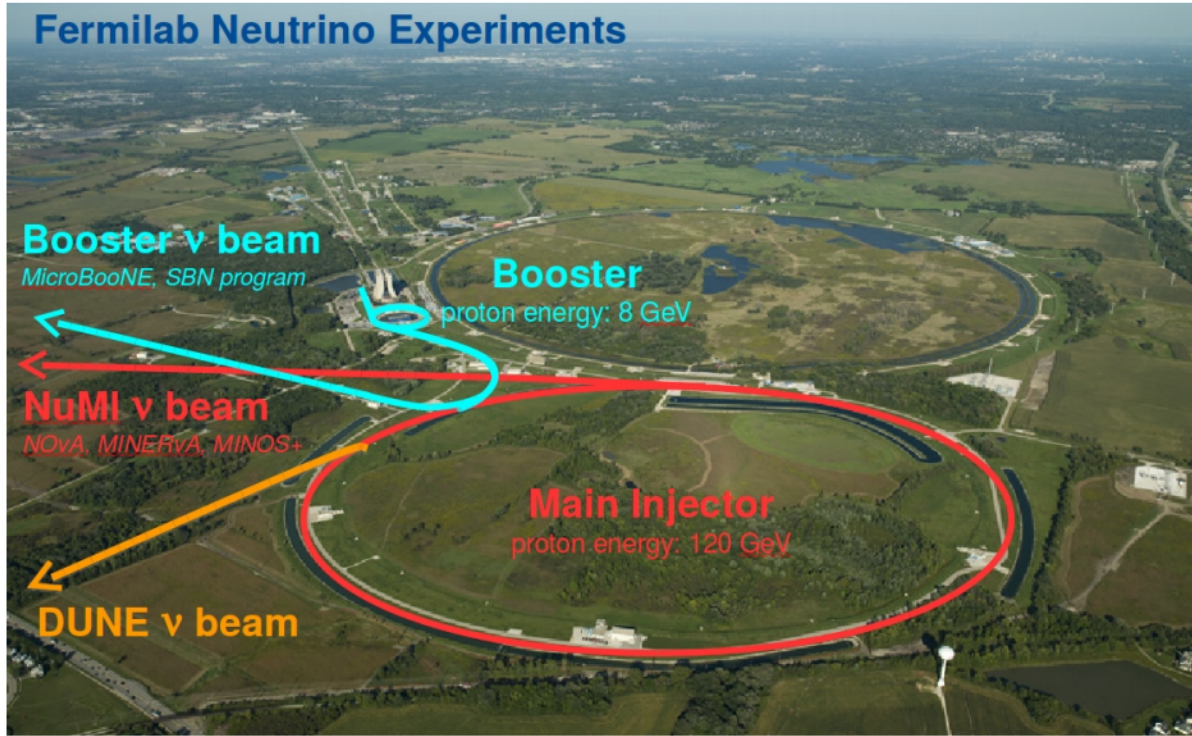


Figure 3.2: Aerial view of the Main Injector and the Booster Neutrino Beam at Fermilab

### 3.4.1 Creating the Booster Neutrino Beam

The BNB is a very pure  $\nu_\mu$  beam, with only 0.6% contamination from  $\nu_e$ s. The energy also peaks around 700 MeV which is desired based on the probability of oscillation equation which depends on the the value of  $L/E$ , where  $L$  is the distance of the detector from the neutrino beam and  $E$  is the energy of the neutrino beam.  $L/E$  was chosen to increase the probability of seeing neutrino oscillations in the MiniBooNE Low Energy Excess (LEE) range based on the probability of oscillation equation, which is  $P_{\nu_\mu \rightarrow \nu_e}(L, E) = \sin^2 2\theta \sin^2 \left( 1.27 \Delta m^2 \frac{L}{E} \right)$ . The BNB collides 8.9 GeV/c momentum protons from the FNAL booster synchrotron into a beryllium target which produces a high flux of neutrinos. The protons originate from  $H^2$  gas molecules that are turned into  $H^-$  ions by a Cockroft-Walton generator shown in figure ???. The  $H^-$  initially are accelerated to 1MeV kinetic energy and are then passed to a linear accelerator using alternating electromagnetic fields to increase their energy to 400MeV. The ions are stripped of electrons by passing them through a carbon foil. The protons are bunched

into beam spills which contain  $4 \times 10^{12}$  protons in a  $1.6 \mu\text{s}$  time window per spill. It's at this point that the protons are directed towards the beryllium target. The amount of protons directed towards the target (POT) is measured by two toroids upstream of the target with an error of 2%. Beam intensity, timing, width, position, and direction are monitored by beam position monitors, multi-wire chamber and resistive monitors. The beryllium target is 71.1 cm long, 1.7 proton interaction lengths, and is 0.51 cm in radius. The target is located inside a larger focusing electromagnet called the horn. The horn is an aluminum alloy pulsed toroidal electromagnet. The pulsed current peaks at 170 kA with a time-width of  $143 \mu\text{s}$  which coincides with the protons arriving on the target. The current flows from the inner conductor to the outer conductor with a maximum magnetic field of 1.5 Tesla. The magnetic field focuses the charged secondary particles produced by the p-Be interactions. The direction of current can be switched to changed to polarity of the secondary particles being focused creating a beam of either primarily neutrinos, with positively charged secondary particles, or antineutrinos.

Further down the beamline is a concrete collimator which absorbs particles not necessary to the neutrino flux. The collimator is 214 cm long and 30 cm in radius. After the collimator comes a 45 meter long, 1 meter radius, air-filled cylindrical decay region which then ends in a beam-stop made of steam and concrete. The beam-stop contains an array of gas proportional counters to detect muons. The BNB is shown in figure 3.3.

## 3.5 Event Reconstruction



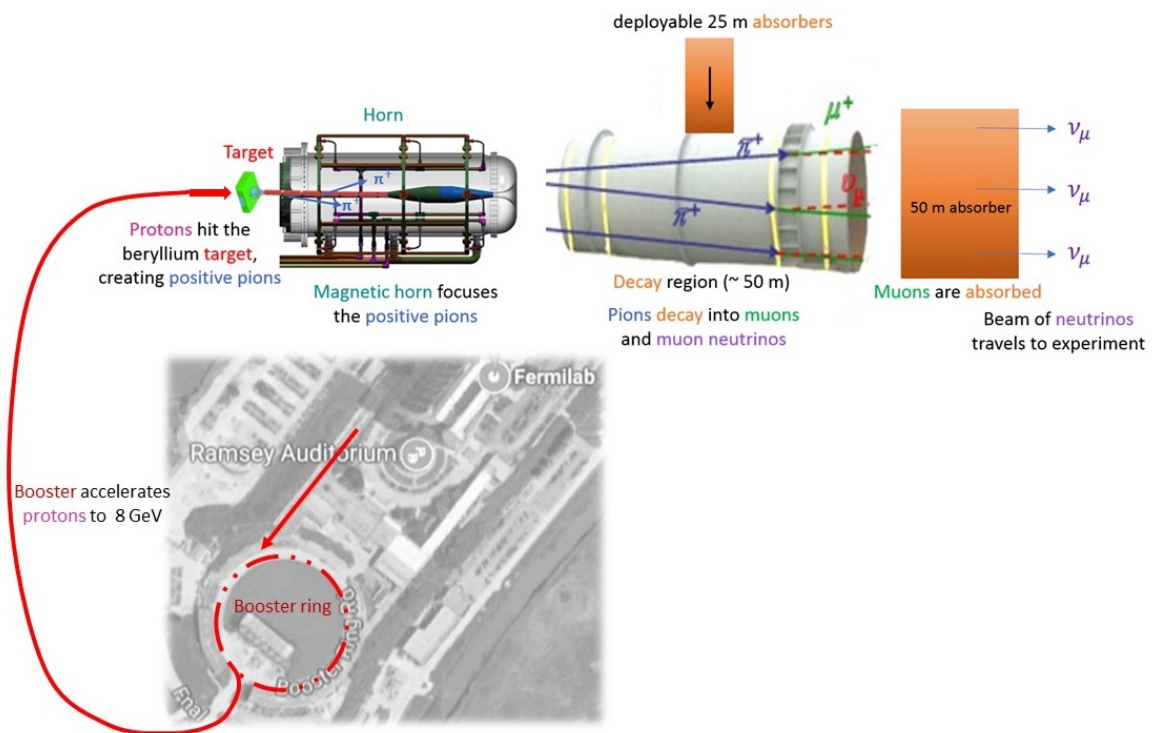
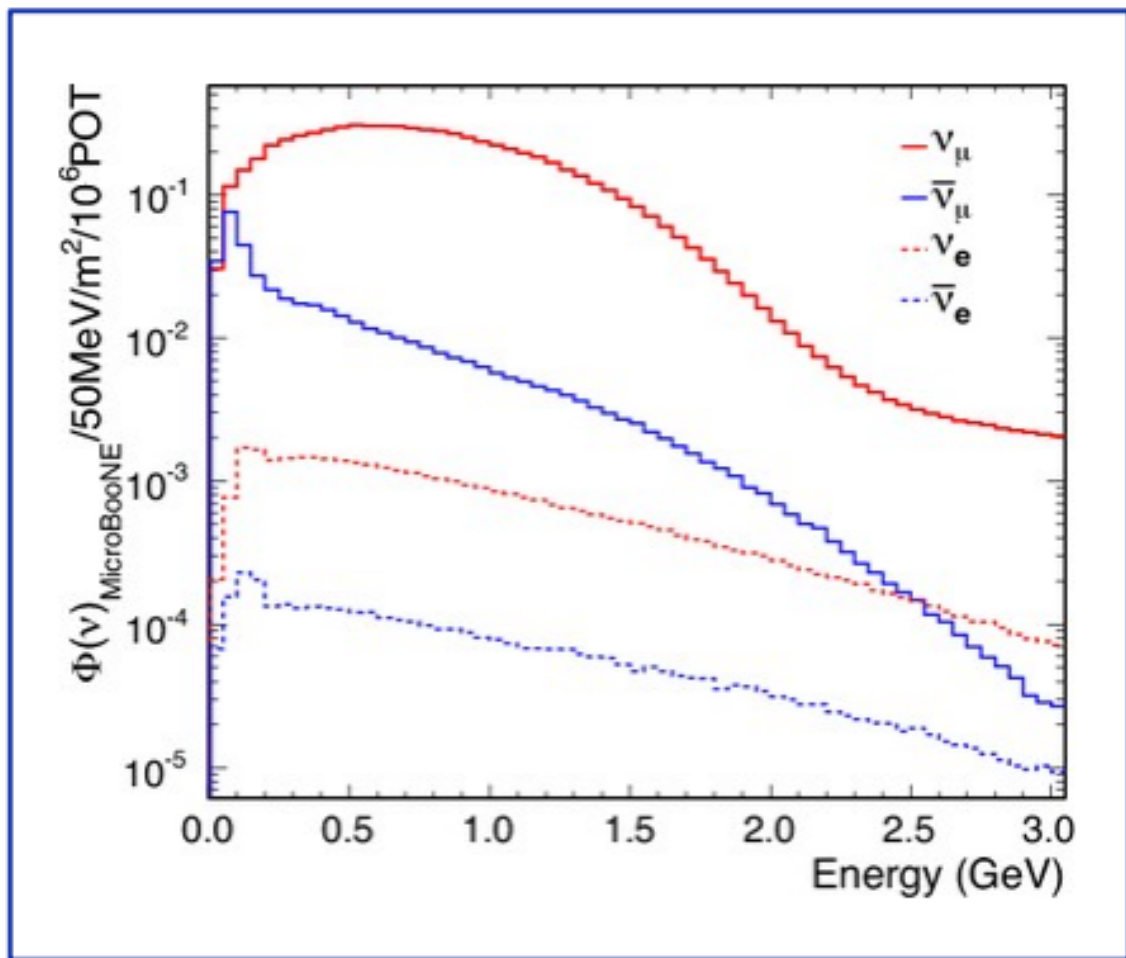


Figure 3.3: Aerial view of the Main Injector and the Booster Neutrino Beam at Fermilab

## BNB Neutrino Flux [simulation]



**Figure 3.4:** Energy spectrum of the Booster Neutrino Beam at Fermi National Laboratories

## Chapter 4

# Neutrino Identification: Finding MicroBooNE's first Neutrinos

The goal of the Neutrino Identification analysis was to positively identify BNB neutrino interactions in the MicroBooNE detector collected during the first days of running. Neutrino event candidates were identified in part by using a cut on detected flash of scintillation light during the 1.6  $\mu$ s beam-spill length of the BNB as well as identifying reconstructed object from the TPC that are neutrino like. After this selection, 2D and 3D event displays were used for verification of the selection performance. This selection was targeted to reduce the ratio of neutrino events to cosmic-only events from the initial 1 neutrino to 675 cosmics to a ratio of 1 to 0.5 or better which is equivalent to a background reduction by a factor of 1000 or more. These selected events were used for MicroBooNE's public displays of neutrino interactions. A clearly visible neutrino interaction with an identifiable vertex and at least 2 tracks originating from the vertex was what the analysis focused on. This analysis wasn't optimized for high purity or efficiency, but rather for very distinguishable neutrino interactions that could be identified by the public.

### 4.1 Flash Finding

Flash finding is the first step used in finding neutrino interactions. This section will detail how optical information is reconstructed as well as analysis scripts and event filters were used.

### 4.1.1 Flash Reconstruction

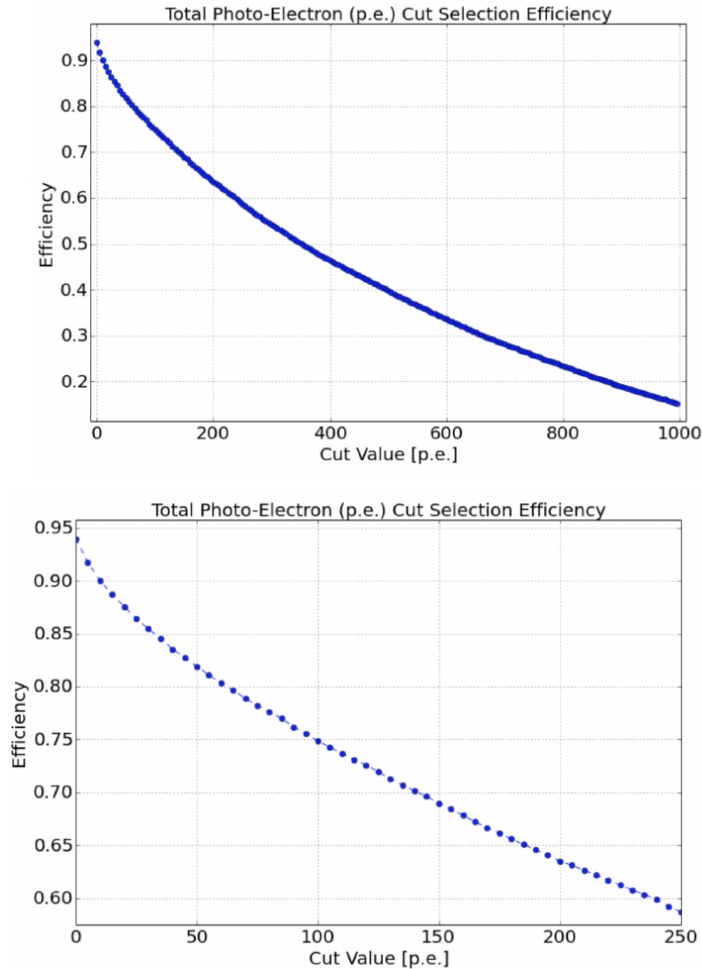
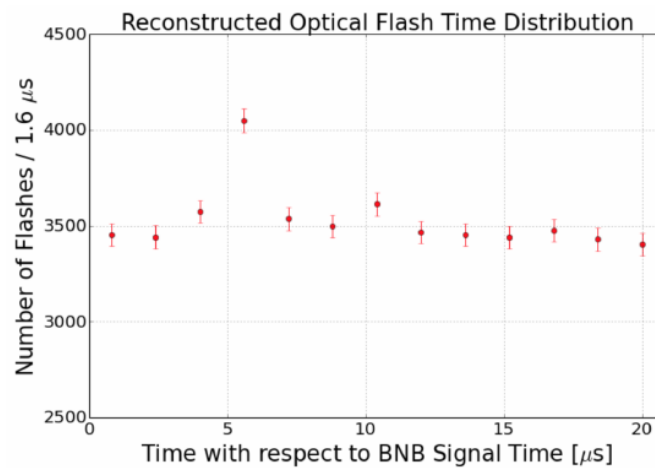


**Figure 4.1:** Efficiency for selecting beam events as a function of minimum total PE cut for all PE cuts as well as zoomed into interesting region.

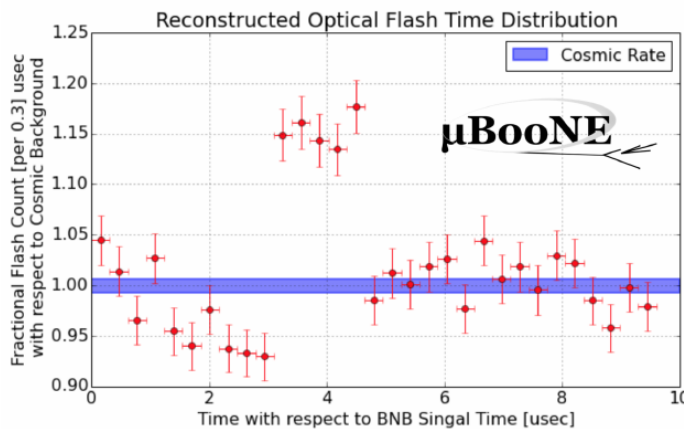
A flash is described as a collection of light seen at the same time within the detector. They are then reconstructed by identifying signal from the PMTs above a specific photoelectron (PE) threshold. These signals are called optical hits. Optical hits from all the PMTs are then accumulated into  $1 \mu\text{s}$  bins of time. If a specific bin is above a set PE threshold, then the optical hits that overlap in time are labeled as the hits from the flash. All flash reconstructed properties like average time and x/y positions are then found via the flash labeled optical hits. The total size of the flash is found by summing up the total number of photoelectrons from all PMTs. Neutrino interactions and cosmic muons will have a larger flash size compared to noise and other low-energy backgrounds, therefore a total PE cut is used to reject these backgrounds. A total PE

cut of 50 PE was deemed sufficient for this analysis. Figure 4.1 show the total PE versus the selection efficiency of selecting neutrino beam events.

### 4.1.2 Beam Timing



(a) Predicted distribution of flash times with respect to trigger time for 1 day of data taking at nominal rate and intensity



(b) Measured distribution of flash times with a 50 PE threshold cut, with respect to trigger time. Shown as a ratio to the expected cosmic rate from off-beam data. A clear excess from neutrinos is visible between 3- 5  $\mu$ s after the trigger time.

It is necessary to get the specific time from flashes if one uses flashes to filter out neutrino interactions coincident with the neutrino beam spill period and background. Before a filter can be applied, an understanding of the timing of the trigger and PMT

readout with respect to the arrival of neutrinos from the BNB. To do this, a  $1.6\ \mu\text{s}$  window near the expected beamtime was created and verified by finding that the number of flashes was significantly above the cosmic-ray background flashes. Beam data during the first week of running, October 16th 2016 through October 22nd 2016 and were used for a timing measurement. The total POT uses corresponds to roughly 24 hours of data taking at nominal intensity ( $4 \times 10^{12}\ ppp$ ) and a 5 Hz repetition rate. Figure 4.2a shows size of the expected neutrino signal in time using Monte Carlo predictions and figure 4.2b shows the neutrino signal in data. The intensity in data is lower, however there can still be seen a significant excess above data.

### 4.1.3 Event Rates

Applying a 50 PE threshold cut inside a  $1.6\ \mu\text{s}$  window reduces the cosmic-ray passing rate to 0.8%. With a 5 Hz beam rate, this corresponds to 135 cosmics passing per hour. The neutrino passing rate for this filter is about 22 events per hour. To further increase the neutrino to cosmic ratio, TPC topology cuts were implemented and will be discussed in the following section.

## 4.2 TPC Topology Selection

In order to further reduce the background of cosmic events, two independent selection streams using TPC wire data reconstruction was implemented. The first using 2D reconstructed clusters, and the second using 3D reconstructed tracks. Both streams look for neutrino interactions in the active TPC volume which are identifiable by two or more tracks originating from the same vertex.

Both 2D and 3D channels were optimized using monte carlo simulation which used a 128 kV cathode voltage. Passing rates were calculated using a 0.008 efficiency factor for cosmic events passing to simulate the flash finding described in section 4.1. This efficiency factor was an overestimation and was just used to get a general feel of what signal and background rates we would actually see in data.

### 4.2.1 Cosmic Tagging

The first step in TPC selection was based on the geometry of cosmic tracks in an event. The cosmic ray muon geometry tagger runs on 3D tracks and assigns a score to each reconstructed track on the likeliness of the track originating from a cosmic. The cosmic scores are detailed below:

- 1: The track is tagged as entering or entering the TPC
- 0.95: The track is a delta ray associated with a tagged track
- 0.5: The track is either entering or exiting, but not both
- 0.4: The track is entering or exiting through the Z boundary
- 0: The track isn't tagged

Clusters are assigned either a 0 or 1, 1 being a cosmic. In simulation, 90% of cosmics are tagged as cosmics. These tracks are no longer considered when looking for a neutrino topology. Requiring that the tracks be contained in turn affects the neutrino efficiency by 20%. The algorithm checks that each track is contained within a boundary region of 10 cm from all sides of the TPC. This boundary region was optimized via handscanning of experimental data.

As can be expected, cosmic tagging is more efficient in the 3D channel (tracks) than the 2D channel (clusters) because the reconstructed tracks can use the full 3D position information of the entering and exiting points while the 2D channel mainly use the reconstructed x position of the cluster which is associated to timing.

Cosmic tagging uses timing information to reject tracks and clusters that are outside of drift window. The drift window for 128 kV is 1.6  $\mu$ s while for 70 kv, the actual voltage MicroBooNE is running at, is 2.3  $\mu$ s. Due to this variation between simulation and data, we expect to see  $2.3/1.6 = 1.44$  times more cosmic induced tracks or clusters in the drift window.

### 4.2.2 2D Cluster Selection

This selection was spearheaded by myself and Katherine Woodruff. After looking at experimental cosmics data, 2D clustering performs well, while 3D track reconstruction is affected by more variations in simulation, for example noise filters. This was the

motivation for having a selection only on 2D clusters in the collection (Y) plane. As stated previously, the goal of this analysis was to find identifiable neutrino interactions for use in public event displays, in future analyses, the 3D track reconstruction has been modified to further increase the tracking efficiency and has more information than just the clusters. For this analysis, however, 2D cluster information was sufficient enough for neutrino selection.

## Primary Cuts

The first cuts were used to select which clusters to consider. First the clusters must have at least ten hits on the collection plane and have a cosmic tagging score  $< 0.4$ . Only events that have at least two clusters that satisfy these primary cuts continue on.

After the initial cosmic tagging is applied, the following cuts are used to further separate identifiable neutrinos for background cosmics.

The next cut was to remove long, vertical clusters. This was applied after seeing that most cosmic induced clusters passing were long with high angles, while neutrino induced clusters were mainly forward going. We required a good cluster to either have a projected start angle less than 30 degrees from the z axis or be less than 200 wires long. The length cut was added to make sure we don't cut any short high angle clusters that can correspond with a proton, or other highly ionizing particle associated with a long muon cluster. The 200 wire cut roughly equates to 0.6 m in the z direction, with a 3 mm wire pitch. Also, the projected angle is defined by  $\tan \alpha = \Delta T / \Delta W$  where T is the time ticks and W is the wires.

The last cut requires the clusters to be either 30 time ticks or 30 wires. This cut was applied to reduce small delta rays associated with a cosmic without removing proton clusters associated with a long muon cluster, which saves ideal neutrino events that have both a long minimum ionizing muon like cluster and a short highly ionizing proton like cluster.

## Secondary Cuts

The secondary cuts look to match long, low-angle clusters with short, high-charge clusters. Only clusters that have passed previous cuts are used. First clusters with length greater than 100 wires are chosen, which is approximately 0.3 m in the z



Cluster set	No Cuts	Primary Cuts	Secondary Cuts
Neutrinos only	570	303	32
Cosmics only ( no flash)	308,016	291,879	602
Cosmics only (w/ flash)	2464	2335	5
Neutrinos/Cosmics	0.23	0.13	6.4

**Table 4.1:** Passing rates for 2D cluster cuts for neutrino on MC set and a cosmic only MC set. First column shows event rates with no cuts applied to both sets. Columns two and three show event rates after primary and secondary cuts are applied. Line three shows the second line scaled with the flash finding factor of 0.008. All events are normalized to per day assuming we are running at 5 Hz.

direction. Then we search for any cluster that is within approximately 3 cm ( 10 wires and 30 time ticks) away from the low-z end of the long cluster. This cluster must also be shorter than the first. In our reconstruction, the start and end point of a cluster can be swapped so both ends of the short cluster are compared to the long cluster.

Now that there is a vertex match, cuts based on charge and projected opening angle are implemented. We require the short cluster to have a higher start charge than the long cluster or the long cluster be longer than 500 wires. Start charge is defined as the charge on the first wire in ADC counts. The projected opening angle must also be between 11 and 90 degrees. This last cut is intended to remove clusters that are entirely overlapping or are part of the same long track. The resulting neutrino/cosmic event rate per day is shown in table 4.1. Figures 4.3 and 4.4 shows the percentages of clusters that pass each primary and secondary cuts.

### 4.2.3 3D Tracks and vertices Selection

The neutrino selection for the 3D channel was based on a reconstructed vertex and two tracks. All vertices and tracks were looped over that had a cosmic tag score  $< 0.4$  and the distances below were calculated:

- $d$ : distance between the start points of the two tracks.
- $d_1$ : distance between vertex and start of track 1.
- $d_2$ : distance between vertex and start of track 2.

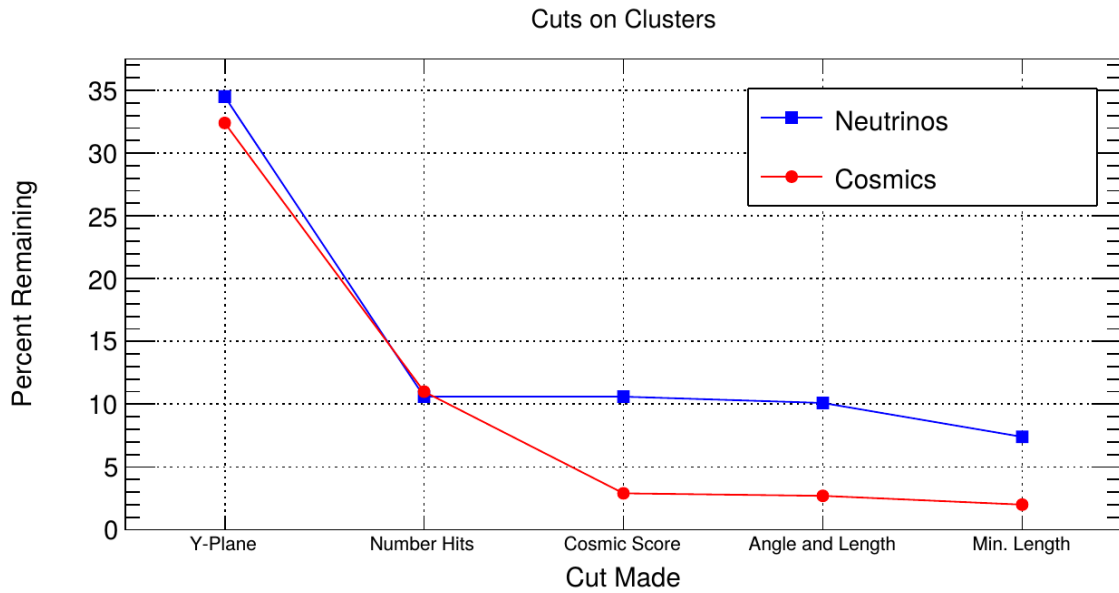


**Figure 4.3:** Percent of good clusters remaining for neutrinos and cosmics after the primary cuts were applied. This is relative to total number of initial clusters.

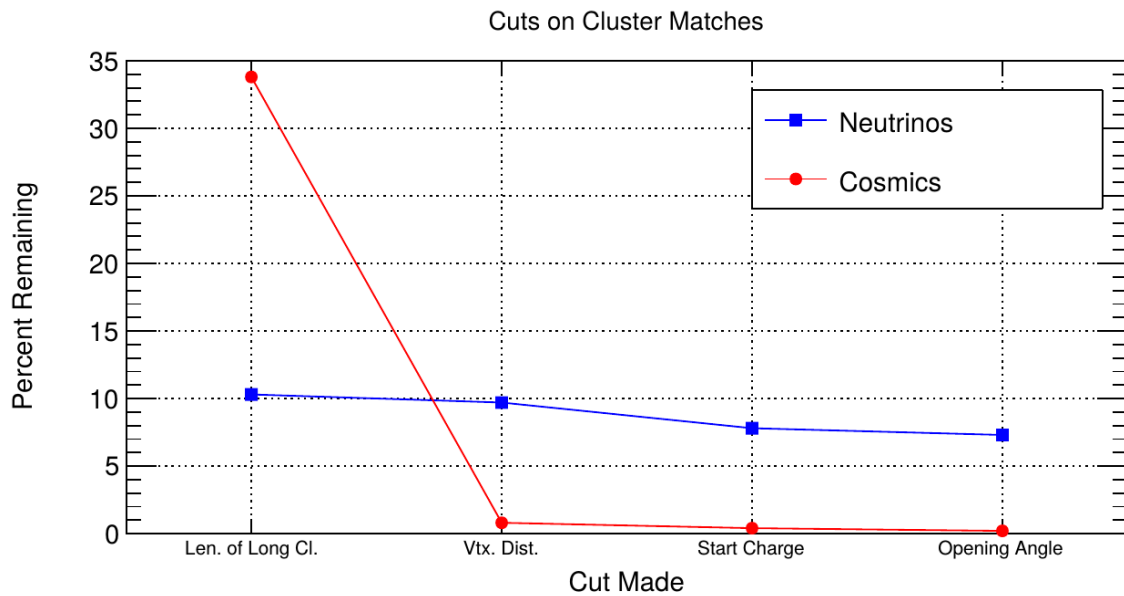


**Figure 4.4:** Percent matched cluster pairs remaining for neutrinos and cosmics after secondary cuts applied. This is relative to the number of events that contain clusters which pass the primary cuts.

The maximum distance of all three is then selected as the important characteristic per trio. The best trio is the one that has the smallest maximum distance. The  $\min(\max_d)$  for all trios in an event were plotted for BNB neutrino events and for cosmics to find the best cut value for each tracking algorithm. The distribution of  $\min(\max_{d,i})$  is smaller for neutrinos than for cosmics. The cut values for different tracking and clustering algorithms are shown below. These cut values were chosen to minimize the cosmic background to 20%.

- trackkalmanhit with cccluster  $\min(\max_{d,i}) < 3$  cm.
- trackkalmanhit with pandoraNu  $\min(\max_{d,i}) < 4.5$  cm.
- pandoraNu with cccluster  $\min(\max_{d,i}) < 5$  cm.

#### 4.2.4 TPC Updates

After doing a visual hand-scanning of the first beam data processed with the filters detailed above, the events passing had a larger contamination of background than expected. This was mainly in part due to the reconstruction performing better on simulation than on data. Due to this, additional cuts on both streams needed to be implemented in order to increase signal/background ratio. These cuts were added on top of the filters described above and further reduce the event count.

#### 2D Filter Updates

The main background observed in the 2D filter were Michel events, where the muon and electron formed two connected clusters. These events were rejected by comparing the start and end charge deposition of the long cluster (i.e muon particle). The start charge deposition must be less than the end charge deposition. This cut is implemented because muons have a higher ionization loss at the end.

#### 3D Filter Updates

It was seen that cosmic tracks can often originate or end at the same point, therefore faking a signal. Cosmic tracks, however, are mostly vertical. By requiring the angle of the longer track have a cosine greater than 0.85 with respect to the z-axis as well

650 as requiring the longer track to have a length greater than 10 cm, we can reduce this  
651 background.

## 652 4.3 Conclusion

653 After processing these filters in parallel, it was shown that the 3D filter had a higher  
654 purity than the 2D filter because of the higher cosmic rejection being used due to 3D  
655 reconstruction. The 2D filter is blind to track entering/exiting from the top or bottom  
656 of the TPC. Although the 3D filter had a higher purity, the 2D filter was still able to  
657 find identifiable events in data that were used as public event displays. A sample of  
658 event displays are shown in figures ?? and ??.

## Chapter 5

# CC-Inclusive Cross Section Selection Filter

The CC-Inclusive cross-section selection I and selection I modified filters used in this analysis will be described in the following sections below. These filters are an expansion of the Neutrino ID filter. The work done in this thesis was to further improve these selections by increasing both efficiency and purity as well as increasing acceptance without further affecting the kinematic distributions of the selected neutrino events.

MicroBooNE requires fully automated event reconstruction and selection algorithms for use in the many physics measurements being worked on to date due to the large data rate MicroBooNE receives. Being able to automatically pluck out the neutrino interaction among a sea of cosmics proved to be challenging but was accomplished. MicroBooNE has developed two complementary and preliminary selection algorithms to select charged-current  $\nu_\mu - Ar$  interactions. Both are fully automated and cut based. The results of this thesis will focus on selection I and selection I modified and will focus on further improving these algorithms using Convolutional Neural Network (CNN) implementations. These selections identify the muon from a neutrino interaction without biasing towards track multiplicity. To combat cosmic and neutral current background, the analysis is strongly biased towards forward-going long tracks which are contained. This limits phase space and reduces acceptance.

## 5.1 Data and MC Processing Chain

The data used for this analysis were based on hardware and software triggers. Events used came from the *BNB\_INCLUSIVE* and *EXT\_BNB\_INCLUSIVE* streams and were used for signal and background. The *BNB\_INCLUSIVE* stream is chosen by requiring that the hardware trigger bit is fired and that the event passed an optical software trigger within a BNB spill timing window. The *EXT\_BNB\_INCLUSIVE* stream requires the EXT hardware trigger to fire as well as pass the same optical software trigger within a BNB spill size timing window similar to the *BNB\_INCLUSIVE*.

The two MC samples used in this analysis and for determining selection efficiencies and purities were GENIE BNB neutrino interactions with CORSIKA cosmic ray overlay within the readout window and inTime CORSIKA cosmic rays. The MC samples generated used *uboonecode v04\_36\_00* and are based on the following packages:

- larsoft v04\_36\_00
- GEANT v04\_09\_06\_p04d
- GENIE v02\_08\_06d
- GENIE xsec v02\_08\_06a
- pandora v02\_03\_0a
- CORSIKA v07\_4003

Both data and MC samples were processed using the same reconstruction release, *uboonecode v05\_08\_00* and the fcl files used for reconstruction are listed below:

- MC fcl files
  - reco\_uboone\_mcc7\_driver\_stage1.fcl
  - reco\_uboone\_mcc7\_driver\_stage2.fcl
- Data fcl files
  - reco\_uboone\_data\_Feb2016\_driver\_stage1.fcl
  - reco\_uboone\_data\_Feb2016\_driver\_stage2.fcl

On top of the hardware and software triggers, the data also had to pass more criteria to be identified as part of the good run list. The criteria is detailed below.

- **Detector conditions:** the detector has to be in a good operating condition. The detector conditions are read from the slow monitoring database and are required to be within the alarm thresholds. The variables of interest for events passing the good run list criteria include DAQ, PMT, HV, Drift HV, wire bias, electron lifetime and detector power. These conditions need to be met on a run-by-run basis in order to pass the selection.
- **Data quality:** normal and stable behavior for basic reconstruction quantities. These reconstruction variables include average number of tracks, hits, and flashes in each event, the average length of tracks, the average amplitude and area of hits, the average PE and the average spread of each one of these quantities.
- **Beam Conditions:** the BNB must be on and stable and the POT per spill needs to be above the intensity threshold. Beam quality conditions include checking the fraction of proton beam interacting within the target, the horn current, and the intensity of protons per spill. The final sample is  $5 * 10^{19}$  and a per-spill intensity of  $4 * 10^{12}$
- **Run processed:** the full run must be processed completely without missing subruns or crashes in the data processing.

## 5.2 Normalization of data and MC

The off-beam sample is used to measure beam unrelated backgrounds. For normalization, one needs the total number of BNB spills ( $N_{BNB}$ ) and the total number of external triggers. The BNB spills used need to pass the beam quality cuts. The normalization factor is then  $N_{BNB}/N_{EXT}$  which is 1.23.

To normalize generated BNB MC events to POT, we used the following:

- $5 * 10^{19} POT = 41524.3$  generated events

where this scaling factor only applies to mcc7 generated events. The inTime cosmic sample is normalized with respect to the open cosmic sample so an understanding of both is necessary. The POT per beam spill for mcc7 BNB samples is  $5 * 10^{12}$ . To calculate how many spills are necessary to produce a specific POT one would multiply the total POT by the average 1/POT per spill. For a total POT of  $5 * 10^{19}$  the amount of spills necessary is  $\frac{5*10^{19}}{5*10^{12}} = 1 * 10^7$ . This is only one in  $\sim 241$  events therefore each

cosmic event needs to be scaled up by a factor of 240.8 when comparing to BNB MC. For inTime cosmics however, two filters are applied to reduce computing and processing time and only leave cosmics that will interact within the detector. The passing rate after these two filters is 0.02125, therefore the total inTime cosmic scaling factor to compare inTime cosmics to BNB is  $0.02125 * 240.8 = 5.12$ .

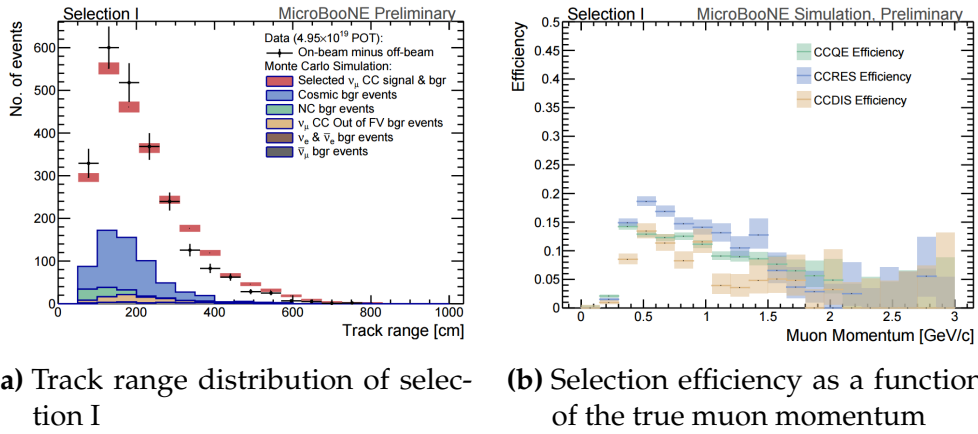


**Figure 5.1:** 5.1a Track range distribution for selection I. The track range is defined as the 3D distance between the start and end of the muon candidate track. No data is shown below 75 cm due to the track length cut described previously. 5.1b Efficiency of the selected events by process quasi-elastic (QE), resonant (RES), and deep-inelastic (DIS). Statistical uncertainty is shown in the bands and the distributions are a function of true muon momentum. The rise of the efficiency between 0 GeV and 0.5 GeV is due to the minimum track length cut and the decreasing efficiency for higher momentum tracks is caused by the containment requirement.

## 5.3 Optical Software Trigger and Reconstruction

### 5.3.1 Software Trigger

Most of the BNB spills from the accelerator do not have a neutrino interaction in MicroBooNE. To save computation resources and reduce data-rates, we require a burst of light in the light collection system in coincidence with the  $1.6 \mu\text{s}$  beam spill. Requiring light activity in coincidence with the beam spill eliminates the vast majority of triggers with no neutrino interaction in the detector, however, it doesn't guarantee the activity in the detector is a neutrino interaction since a cosmic ray can interact in coincidence with the beam spill as well.



To implement this, a software trigger was used on the PMT waveforms to decide whether or not to keep that event. The software trigger is implemented after the event builder combines data from the PMTs and triggers into a single event. The software trigger uses the digitized output of the 32 PMT channels in the light collection system. Only the waveform region in coincidence with the beam spill is used to search for possible triggers. For each PMT, a waveform is found by taking the difference of ADC values is calculated between  $t$  and  $t + s$ . This waveform is then scanned for ADC values above a threshold  $X_0$ . Once an ADC is above this threshold, a discriminator window is opened for a fixed number of time ticks ( $W_0$ ). If the ADC count within this window  $W_0$  is greater than a second larger threshold  $X_3$ , a final window of width  $W_3$  is opened. The max ADC value within this final window is set as the peak amplitude for the PMT and then summed across all 32 PMTs and set to the variable PHMAX. The software trigger places a final cut on the PHMAX variable to decide whether or not to keep the event. The thresholds were found by the Trigger task force using Monte Carlo Studies and are as follows:

- $X_0 = 5$  ADC
- $X_3 = 10$  ADC
- $W_0 = 6$  Ticks
- $W_3 = 6$  Ticks
- PHMAX cut = 130 ADC

### 5.3.2 Flash Reconstruction

MicroBooNE collects light from each of the 32 PMTs either in a continuous readout window of 23.4  $\mu$ s activated by a beam gate signal on the trigger board, or in discriminated pulses of  $\sim 1$   $\mu$ s duration activated if the ADC count for any PMT goes above 80 ADC count. These two formats are saved as output waveforms and put onto an event. Additionally, each PMT can provide two output streams, high-gain ( $\sim 20$  ADC/PE) and low-gain ( $\sim 2$  ADC/PE) channels. The first step in the reconstruction is to merge both these channels into a “saturation corrected waveform” which uses information from the low-gain waveform to correct for saturating high-gain pulses.

The saturation corrected waveform in the continuous readout window is used to reconstruct optical hits. Each PMT’s waveform is scanned for hits then a threshold

based hit reconstruction algorithm is applied which requires pulses of a minimum area in order to be reconstructed. Each reconstructed hit is associated to a PMT, a time in  $\mu\text{s}$ , and a PE count.

Once hits are reconstructed for all 32 PMTs, all PMT information is then combined into optical flashes which represent optical information seen by the PMTs from interactions in the detector. Each flash has information on total light seen per interaction, the distribution of the light across all 32 PMTs, the flash time with respect to the trigger time of the flash, and lastly, the spacial information of the flash in Y-Z plane of the detector. These flashes are reconstructed by requiring that there is a  $\sim 1 \mu\text{s}$  coincidence between the reconstructed hits in all 32 PMTs. The total PE is summed up among all coincident hits across the PMTs and if the total PE is greater than 2 PE, a flash is reconstructed. There are also safe guards in place to take care of late scintillation light.

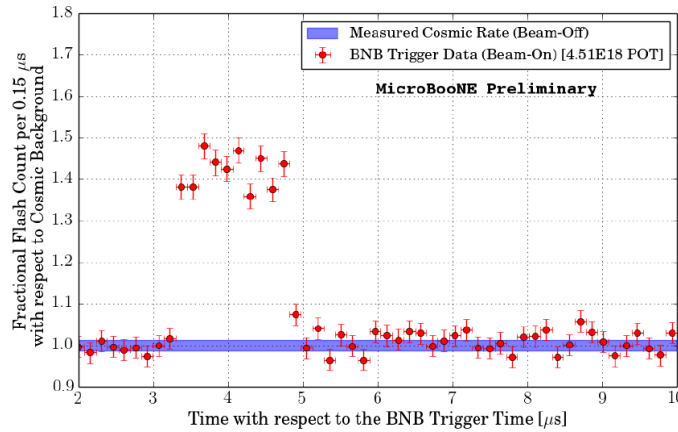


**Figure 5.2:** Time distribution of reconstructed optical flashes with a PE value of 50 or more for a sample of BNB unbiased triggered events.

Figure 5.2 shows the time distribution of reconstructed optical flashes using the BNB continuous stream. You can see a clear excess in coincidence with the expected arrival time of neutrinos. The same flash reconstruction that was used in the cc-inclusive filter detailed here was used to create this plot in data.

### 5.3.3 Beam Window

Figure 5.3 shows the distribution of flashes for on-beam, off-beam and various MC samples. The software trigger has been applied to these samples. The pile-up seen just after 0  $\mu\text{s}$  is a feature of the flash finding algorithm and consists of low PE flashes and

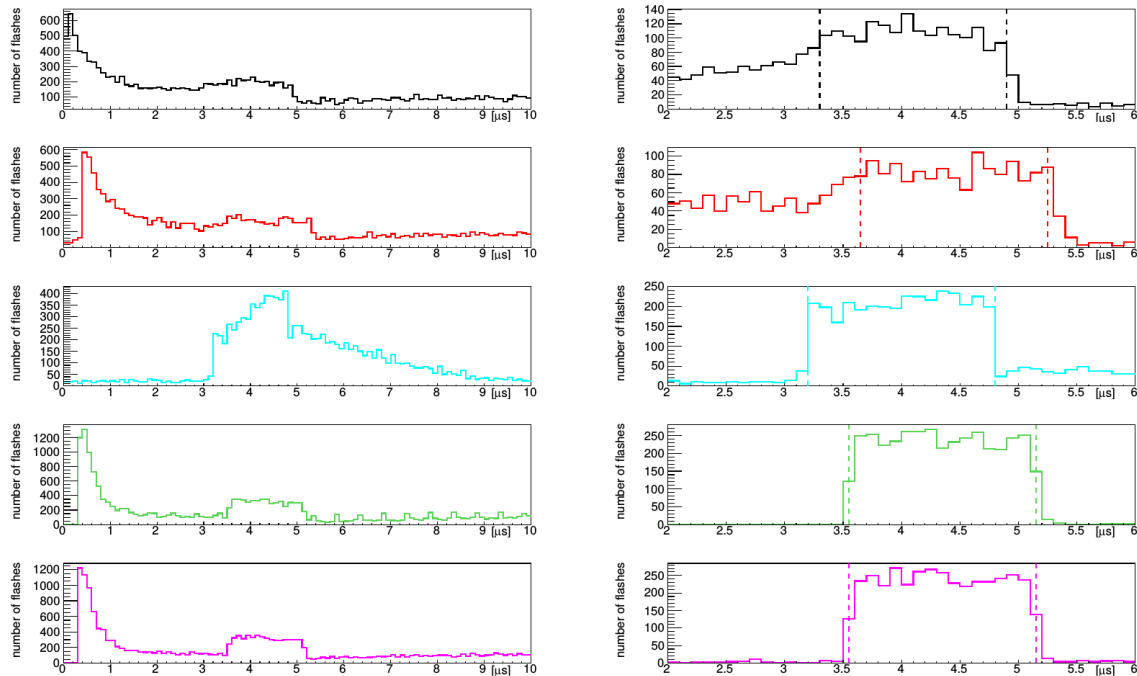


**Figure 5.3:** Flash time distribution for all flashes (left plot) and flashes  $> 20\text{PE}$  (right plot). The different curves are as follows: on-beam data (black), off-beam data (red), CORSIKA inTime MC (light blue), BNB only MC (green), and BNB+Cosmic MC (purple). The dashed vertical lines mark the time window that was chosen for each sample

is removed in the second column of distributions with a low 20 PE threshold cut. The plots show that the time window for the distributions are shifted a small amount from each-other. This is caused by different hardware configurations per sample. Using these distributions, the windows chosen per sample are as follows:

- On-Beam: 3.3 to 4.9  $\mu\text{s}$
- Off-Beam: 3.65 to 5.25  $\mu\text{s}$
- CORSIKA inTime: 3.2 to 4.8  $\mu\text{s}$
- BNB only: 3.55 to 5.15  $\mu\text{s}$
- BNB+Cosmic: 3.55 to 5.15  $\mu\text{s}$

Each window has a width of 1.6  $\mu\text{s}$ .

## 5.4 TPC Reconstruction

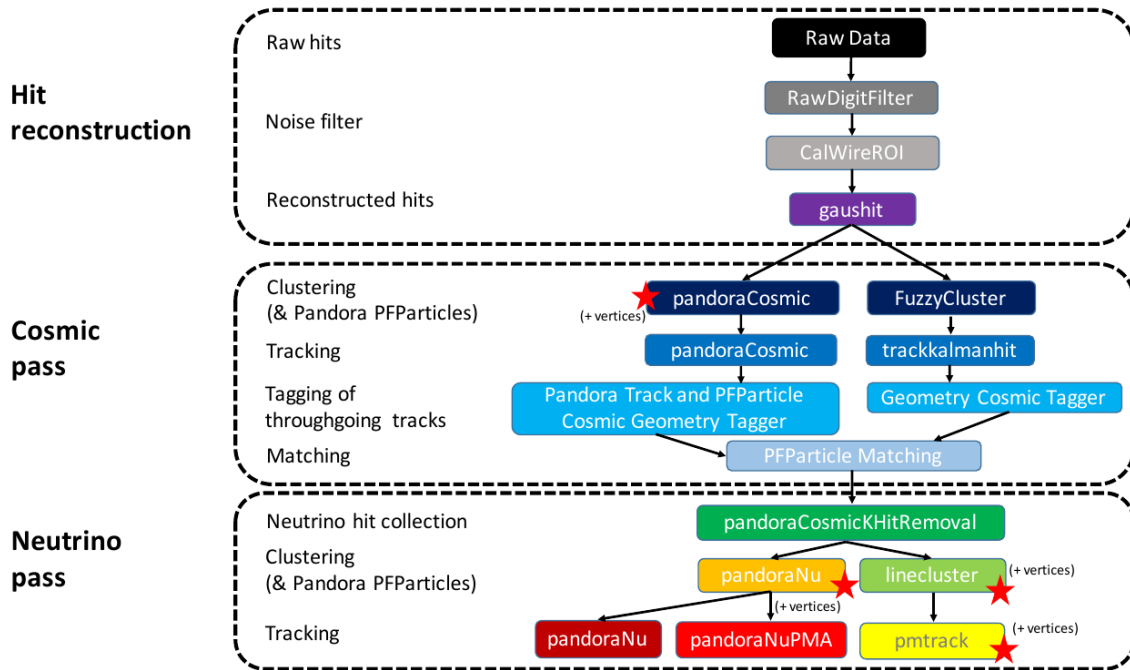


**Figure 5.4:** Reconstruction chain run on both data and MC. The red stars mean that the algorithm returns reconstructed 3D vertices.

Figure 5.4 summarizes the reconstruction chain applied to both MC and data for this analysis. After the hit reconstruction, a cosmic pass is applied which removes all hits associated to through-going tracks. A description of these TPC reconstruction algorithms will be detailed below.

### 5.4.1 Hit Reconstruction

The waveforms used for hit reconstruction consist of charge deposited on the sense wire in drift time. The first step in hit reconstruction is to pass the waveforms through a filtering algorithm to filter out the noise introduced from the electronics. The input waveforms are also truncated from 9600 time ticks to 6400 time ticks in this first step to reduce the data footprint of these waveforms.

Once noise filtering is complete, a deconvolution algorithm is applied to the waveforms to remove the drift field and electronics response, therefore leaving only the ionized electrons kicked off the argon atoms by an incident track. During this process, Region of Interests (ROI) are identified and cut out of the waveforms to further reduce the data volume.

The hit finding algorithm then finds candidate peaks in these ROI's and fits the peaks to Gaussian curves. These Gaussian shaped peaks are now called hits and represent the charge deposition on a wire by the incoming track. These hit objects have a peak time and width and are the basic object input to further algorithms down the reconstruction chain.

### 5.4.2 Clustering

There are multiple clustering algorithms used in this analysis. The main purpose of all the clustering algorithms is to associate hits together in 2D space to create objects like tracks, vertices and showers. For the fuzzy cluster algorithm, three steps are used to achieve this. The first step is to associate hits to each-other using a fuzzy clustering algorithm which gives each hit a degree of belonging to the cluster. Second, a Hough transform is used to find hits associated to candidate tracks and showers within each of the clusters found in the first step. The last step merges smaller candidate tracks and showers into large clusters. The last step also associates unclustered hits into

nearby objects which helps shower reconstruction. The result is a set of clusters made up of associate hits that represent tracks or showers per plane.

The pandora algorithm utilizes it's own clustering algorithm and will be detailed in the next section. The last clustering algorithm is called linecluster. The linecluster algorithm reconstructs 2D linear clusters per plane by fitting a line onto nearby hits which is then extrapolated to neighboring wires. 2D vertices are found per plane by using the intersection points of the ends of nearby clusters. These 2D vertices are then matched in time across all three planes to get a 3D vertex in space.

### 5.4.3 Pandora

### 5.4.4 Trackkalmanhit

The trackkalmanhit algorithm takes 2D clusters returned from the fuzzy cluster algorithm and outputs track objects. There are no hierarchy structure as it is in pandora, each track is independent. There also is no vertex reconstruction with this algorithm as well.

### 5.4.5 Cosmic Hit Removal

The Pandora algorithm is applied to the events twice, the first to remove downward going tracks primarily from cosmic ray muon like particles. The second pass only runs on a subset of hits that aren't associated with cosmic ray muon tracks.

After the first pass, the output of PFParticle hierarchy is then passed to a cosmic ray tagger to look through all hits to determine start and end points. If the start or end point trajectories are consistent with entering or exiting the TPC, then these hits are removed from the second pass. Hits are considered entering or exiting the TPC if the drift time are outside of the neutrino drift window or outside of the fiducial volume of the TPC. The fiducial volume was based on a montecarlo study and is 20 cm from the top or bottom of the TPC and 10 cm from the TPC ends. Hits associated with candidate cosmic ray tracks are removed from the input hit collection and the remaining hits are passed to the neutrino optimized pass of Pandora.

### 5.4.6 Projection Matching Algorithm

The projection matching algorithm (PMA) was inherited from ICARUS and has been implemented in LArSoft. PMA differs from traditional LArSoft 3D reconstruction algorithms. Most 3D reconstruction attempts to match 2D objects from all three planes by drift time, while the PMA algorithm projects a track hypothesis on each plane then the distance between this projection and the hits on each plane is minimized simultaneously. More information can be found in [?].

## 5.5 Event Selection

The first requirement for selecting  $\nu_\mu$  CC events is that the event has at least one scintillation light flash in the beam trigger window with more than 50 PE on all PMTs combined. From the flashes that pass, the most intense is chosen and considered to be originating from a neutrino interaction and will be the only flash used in further cuts.

Vertices are then required to have at least one reconstructed track start or endpoint within a 5 cm radius. Showers associated with a vertex do not pass this cut. All tracks associated with a vertex are then used to calculate a track length weighted average of the  $\theta$ -angle. Of all the vertices that do pass, only the vertex with the most forward going  $\theta$ -angle average of all associated tracks is considered the neutrino vertex candidate. The most forward going  $\theta$ -angle average is chosen by picking the largest track range weighted average of  $|\cos(\theta)|$ , seeing as  $\cos(\theta) = 1$  is the beam direction. Next, it is required that the reconstructed neutrino vertex candidate be within the fiducial volume as well as within the drift time starting at  $t_0$ . The fiducial volume boundaries chosen are 10 cm from the edges of the TPC in x and z which is the drift direction and beam direction respectively, and 20 cm from the edges of the TPC in y which is the vertical direction. For all further cuts, only the longest track associated with the neutrino vertex candidate and this track is assumed to be the muon candidate of the neutrino event.

The next cut requires the position of the flash in the z-direction and the track z-projection to be compared. This basic flash matching algorithm is rudimentary and a placeholder for a more sophisticated algorithm. The z-position of the flash needs to be within 80 cm to the z-positions of track start or endpoints. If the flash is between the track start and endpoint, the distance of the flash to the track is considered to be 0 cm.